Multichannel on-chip data transmission with InGaN/GaN multiple quantum wells devices

Feifei Qin

qinfeifei@njupt.edu.cn

Nanjing University of Posts and Telecommunications

Jiaqi Wu

Nanjing university of posts and telecommunication

Xueyao Lu

Nanjing university of posts and telecommunication

Xiaoxuan Wang

Southeast University

Qingsong Jiang

Huaiyin Institute of Technology

Daotong You

Jinan University

Yang Chen

Nanjing university of posts and telecommunications

Yue Cao

Nanjing university of posts and telecommunications

Lei Zhang

Nanjing University of Posts and Telecommunications

Junfeng Lu

Nanjing University of Aeronautics and Astronautics   https://orcid.org/0000-0001-6458-7734

Gangyi Zhu

Nanjing

Yongjin Wang

Grünberg Research Centre, Nanjing University of Posts and Telecommunications
https://orcid.org/0000-0001-8109-4640

Article

Additional Declarations: There is no conflict of interest

Multichannel on-chip data transmission with InGaN/GaN multiple quantum wells devices

Feifei Qin[1*], Jiaqi Wu[1], Xueyao Lu[1], Xiaoxuan Wang[2*], Qing-song Jiang[3], Daotong You[4], Yang Chen[1], Yue Cao[1], Lei Zhang[1], Junfeng Lu[5], Gangyi Zhu[1*], Yongjin Wang[1]

[1]GaN Optoelectronic Integration International Cooperation Joint Laboratory of Jiangsu Province, College of Telecommunications and Information Engineering, Nanjing University of Posts and Telecommunications, Nanjing, 210003, China;

[2]State Key Laboratory of Digital Medical Engineering, Southeast University, Nanjing 210096, China·

[3]Faculty of Electronic Information Engineering, Huaiyin Institute of Technology, Huai'an 223003, China

[4]Institute of Photonics Technology, College of Physics and Optoelectronic Engineering, Jinan University, Guangzhou 510632, Peoples Republic of China,

[5]College of Physics, MIIT Key Laboratory of Aerospace Information Materials and Physics, Key Laboratory for Intelligent Nano Materials and Devices, Nanjing University of Aeronautics and Astronautics, Nanjing 211106, China

*Corresponding author:

qinfeifei@njupt.edu.cn, wxxseu@seu.edu.cn , zhugangyi@njupt.edu.cn

Abstract:

The high-speed, low-noise on-chip data transmission system holds significant application prospects in fields such as communications, artificial intelligence, and optical sensing. However, a sapphire-based device hinders the development of multichannel and on-chip data transmission due to its drawbacks in optical loss and crosstalk. Herein, we propose a novel InGaN/GaN multiple quantum wells (MQWs) based transceiver array (5×3) on a silicon platform for data transmission. Each communication unit comprises a coupled structure of a circular emitter and a square receiver. The InGaN/GaN device operates with emission spectra in the range of 475

nm to 575 nm, optical response spectra from 350 nm to 500 nm, fast response times (rise/decay) of 31.34/27.56 μs, and high system communication bandwidth of 15.34 kHz. An open-eyed diagram of the communication unit is realized at a data rate exceeding 0.7 Mbps; thus, the overall data rate of the chip can be estimated to exceed 10.5 Mbps. Interestingly, experimental and simulation results indicate that the well-designed 3-micron intra-unit coupling distance and a 1 mm device spacing ensure that the communication channels can operate independently and are insensitive to inter-channel and environmental interferences, including extraneous sound signals and daylight. Finally, we demonstrate a two-channel communication process. One channel carried text information in ASCII code format, specifically the "NJUPTB20012616," while the other transmitted image information after being quantized into 0-255 gray coordinates. This scalability offers significant potential for high-capacity communication systems on a single chip, making it a promising solution for integrated optoelectronic applications.

1. Introduction

Si-based photonics and optoelectronics, with their large-scale and low-cost fabrication technology, are a crucial cornerstone in the realization of optical interconnects and photon-electronic integrated circuits[1, 2]. In recent years, optoelectronic chips based on GaN materials have also shown significant application prospects in communication, artificial intelligence, quantum computing, and sensors, owing to their advantages in process compatibility, device stability, gain adjustability, low power consumption, and electromagnetic compatibility[3-6]. Meanwhile, GaN chips are being pushed to evolve in the direction of low cost, small size, and high-speed performance with integrated designs. In recent reports, coupled devices such as GaN-based chips on silicon-on-insulator (SOI) substrates, silicon nitride, and sapphire substrates[7-10] have been designed and fabricated. For example, Chen et al. present an AlGaN multiple quantum wells (MQWs) diodes via concentric ring-circle configuration; it shows an improvement in the ratio of emitter injection current to detector output photocurrent and higher output photocurrent under the same work mode, providing a plausible approach to achieve low power consumption and high bandwidth in the monolithic integrated optoelectronic chips[11]. Feng et al. propose an integrated sensor that combines an optical source and four photodetectors, which can be used to detect vector forces[12]. However, high interference within the film and in the environment usually leads to crosstalk and high challenges in signal demodulation, particularly in multichannel optical communication systems and highly integrated photonic or optoelectronic systems. When light signals from different sources and with distinct destinations couple and interfere, the communication of the entire chip or even the whole system can be severely affected. Due to the transparency of sapphire, it not only fails to suppress the inherent optical loss in the vertical direction but also introduces new crosstalk, known as crosstalk, through the sapphire propagation path[13]. Although techniques such as laser lift-off to remove sapphire substrates[14] and using an air-cavity patterned sapphire substrate as a light filter can help suppress optical crosstalk, these methods involve high costs or complex design processes.

Compared to other materials, the advantages of Si-based GaN are evident in the design of new integrated transceiver products. On the one hand, it offers excellent compatibility, stability, scalability, and optical properties, and silicon substrates help to isolate crosstalk and signal loss between devices. On the other hand, the MQWs structure of GaN offers the ability to cover the entire optical region and to have a high overlap between the emission spectra and response spectra. GaN-based MQWs diodes can not only function as a light-emitting diode (LED) to generate light but also

function as a photoelectric detector (PD) to detect light[15-17]. These features make Si-based GaN one of the most promising materials for integrated optoelectronic chips. For example, Miyoshi et al[18]. demonstrated real-time optical communications using high-speed and on-chip graphene blackbody emitters by remote heat transfer, the high-speed light emission with a response time of ~100 ps. Pan et al[19]. report an optoelectronic array for in-sensor computing by integrating photodiodes with resistive random-access memories (RRAMs), highlighting the potential of the optoelectronic array as an energy-efficient in-sensor computing primitive for future optical communication applications.

In this work, we demonstrate a large-scale and on-chip integration of GaN emitter and receiver coupled array with 15 pairs of individual communication units on a Si wafer. Each unit is a coupling device that consists of circular receivers and a rectangular emitter. The Si substrate can isolate crosstalk through substrate propagation paths, and the design of a 3-micron intra-unit coupling distance and a 1mm device spacing successfully enables low-interference, multi-signal transmission. We comprehensively characterized the material composition, optoelectronic properties, and communication performance of each device. The emission and detection spectra overlap, ensuring optical communication. Fast response times (rise/decay) of 31.34/27.56 µs and a high system communication bandwidth of 15.34 kHz were realized. It supports on-chip data transmission with a data rate of over 0.7 Mbps per channel and a total data rate of over 10.5 Mbps. Furthermore, our device is insensitive to noise interference during comparative signal transmission tests in different environments (specifically, noise-free, self-interference, daylight, and daylight with sound interference). Finally, we successfully incorporated this chip as a channel unit into a communication system and completed the prototype, enabling data transmission of text, images, and other information.

2. Results and Discussion

2.1 Device design and fabrication

The energy band bending in MQWs devices results in a specific superposition of the emission and absorption spectra, leading to the coexistence of luminescence detection[20,21]. To realize on-chip multichannel communication, 15 pairs (5×3 array) of transceiver units were integrated on a Si platform. As schematically illustrated in Fig. 1(a), for an individual communication unit, data can be input into the square emitter via an electrical signal, which emits an optical signal carrying the information. The circular

receiver then collects the optical signal and converts it back into an electrical injection for light output. By controlling the distance between units (device coupling spacing of 3 μm and a unit distance of 1 mm), the receiver can collect the signal only nearby and avoid crosstalk. The domain part of the communication unit comprises the coupling structure of circular and square InGaN/GaN MQWs, which function as transceivers (Fig. 1(b)). From top to bottom, the structure includes layers of Au, p-GaN, MQW, n-GaN, buffer, and Si layers. The insets in Fig. 1(b) illustrate the physical mechanism of photon emission and detection, establishing a connection between the intimate relationship of optical information in the same MQWs structure of the LED and the PD.
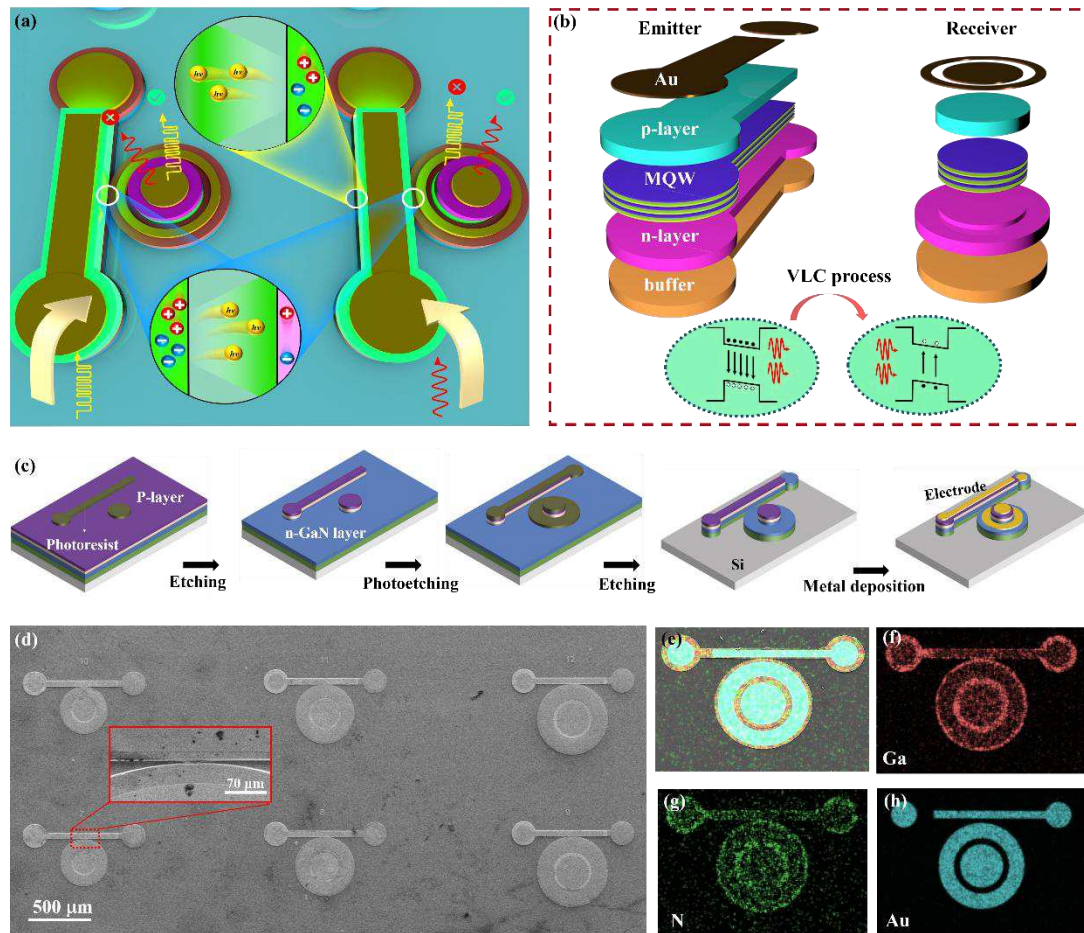

Fig. 1(a) Schematic diagram of the multichannel transmission process: Data will be modulated via MCU, inputted to the chip, and demodulated to the terminal through an optical-electrical-optical conversion process. (b) Schematic diagrams of the device structure and working principles. (c) fabrication process of an individual coupled unit. (d) SEM of the coupled device arrays, the enlarged image shows the gap area. (e-h) EDX elemental mapping of individual single devices.

Due to the integrated characteristics of the MQWs devices, each pair of units can form a communication channel with signal modulation and amplification. The coupled units used in this work are fabricated from Si-based InGaN/GaN MQW devices utilizing standard microfabrication technology. Similar to our previous work [16,22], the integrated optoelectronic chip in this study is realized through photolithography, inductively coupled plasma (ICP) etching processes, and metal deposition, as shown in Fig. 1(c) and the experimental section.

2.2 Structural and morphological characterization

Fig. 1(d) illustrates the scanning electron microscope (SEM) image of the as-fabricated structure used for multichannel simultaneous transmission. The integrated optoelectronic chip in this work contains 15 pairs of devices with identical structures. For each unit, the receiver has a diameter of approximately 385 μm, and the emitter is 1 mm in length and 50 μm in width. The enlarged view displays the coupling gap between the device's parts, which is approximately 3 μm. Details of the individual device and the electrode structure are shown in Fig. S1. The p-type and n-type electrodes are marked, and a gap (approximately 30 μm) is maintained between the two electrodes to prevent short circuits. Fig. 2(e-h) shows the energy dispersive spectroscopy (EDX) elemental mapping analysis of individual single devices, characterizing the distribution of Ga, N, and Au elements in the device (the Au element is mainly distributed in the electrodes). A clear gap is visible for the Au electrodes in Fig. 1(h). XRD, Raman, and PL measurements were used to further confirm the material characteristics of the device. Fig. S2(a) presents the XRD pattern of the integrated optoelectronic chip, where two peaks are located at 27.8° of silicon (111) characteristic peak[23] and 34.0° of GaN (0002) characteristic peak[24]; The Raman spectrum of a single device is shown in Fig.S2(b), where two characteristic peaks correspond to the silicon peak at 518.3 cm^{-1}, compared to the intrinsic peak of silicon at 521 cm^{-1}and the GaN peak at 565.5 cm^{-1}, compared to the intrinsic peak of GaN at 568 cm^{-1}. The consistency of their shifts indicates the presence of stress in the sample itself [25, 26]. Fig. S2(c) shows the photoluminescence spectrum of the device, where the two leading emission bands correspond to the GaN and MQW emission spectra [16].

These characterizations confirm that the device composition is consistent with the chip design and the XRD results.

2.3 Photodetector characteristics of the device

For photonic integrated devices with transmission and reception features, the electroluminescence (EL) spectrum at the transmitting terminal and the detector performance at the receiving terminal are important issues. Additionally, the inevitable interferences that occur during the communication process play a crucial role in evaluating the quality of communication. Our communication unit can be divided into two parts: one is the circular receiver, and the other is the square emitter. Fig. 2(a) shows the EL spectrum corresponding to the emission part under different driving currents, as well as the photoresponsivity spectrum of the receiving part. The InGaN/GaN devices operate with emission spectra in the range of 475 nm to 575 nm and optical response spectra in the range of 350 nm to 500 nm. The two spectra exhibit significant overlap, indicating that the light emitted by the emitter can be received by the receiver, thereby establishing a communication channel. As demonstrated in Figs. 2(a) and 2 (b), the turn-on voltage is ~2.46 V. The EL intensity increases with the driven current, and the sensitivity decreases with the addition of wavelength, with peak values near 356 nm and 0.065 A/W (Fig. S3). The presence of multiple peaks in Fig.2(a) indicates the existence of an interferometric fringe in the emission region. The chromaticity coordinates are (0.2116, 0.7223) in the CIE 1931 chromaticity diagram (Fig. 2(c)).

Fig.2(d-h) shows the optical detection characteristics of the receiver part. For different driven currents of the emitter, the current-voltage (I-V) curves of a single device, acting as a receiver, in Fig. 2(d) indicate that the photocurrent is in the nA range and increases with the addition of illumination. Fig. 2(e) shows the periodic response current of the receiver under different periodic emission light intensities. As the light intensity increases from 132 nW to 750 nW, the response current of the microdisk also increases from approximately 4 nA to about 25 nA. Fig. 2(f) displays the transient light response time of the communication unit. This is defined as the time required for the increase in photocurrent to drop from 90% to 10%; the rise time is ~31.34 μs, and the downtime is ~27.56 μs. These parameters are significantly higher than those of standard GaN-based

devices under out-of-chip conditions[27-29]. Fig. 2(g) and Fig. 2(h) display the frequency responses of the emitter and receiver. It can be seen that as the operating frequency increases to 483 kHz, the -3 dB point is reached, meaning the emission power drops to half of the input power, while the -3 dB point of the receiver is at 15.34 kHz. To further demonstrate the date transmission properties, eye diagrams are used to record units with on-chip data transmission. The observed eye diagrams are inserted in Fig. 2(h) and Fig. S4, where the eye width decreases gradually with an increase in the communication rate, but the eye height remains stable for data rates over 0.7 Mbps. Considering that there are 15 pairs of communication units, the total data rate of the chip can exceed 10.5 Mbps. This data transmission rate is high enough for typical applications, such as serial communication and audio and video transmission[30,31].
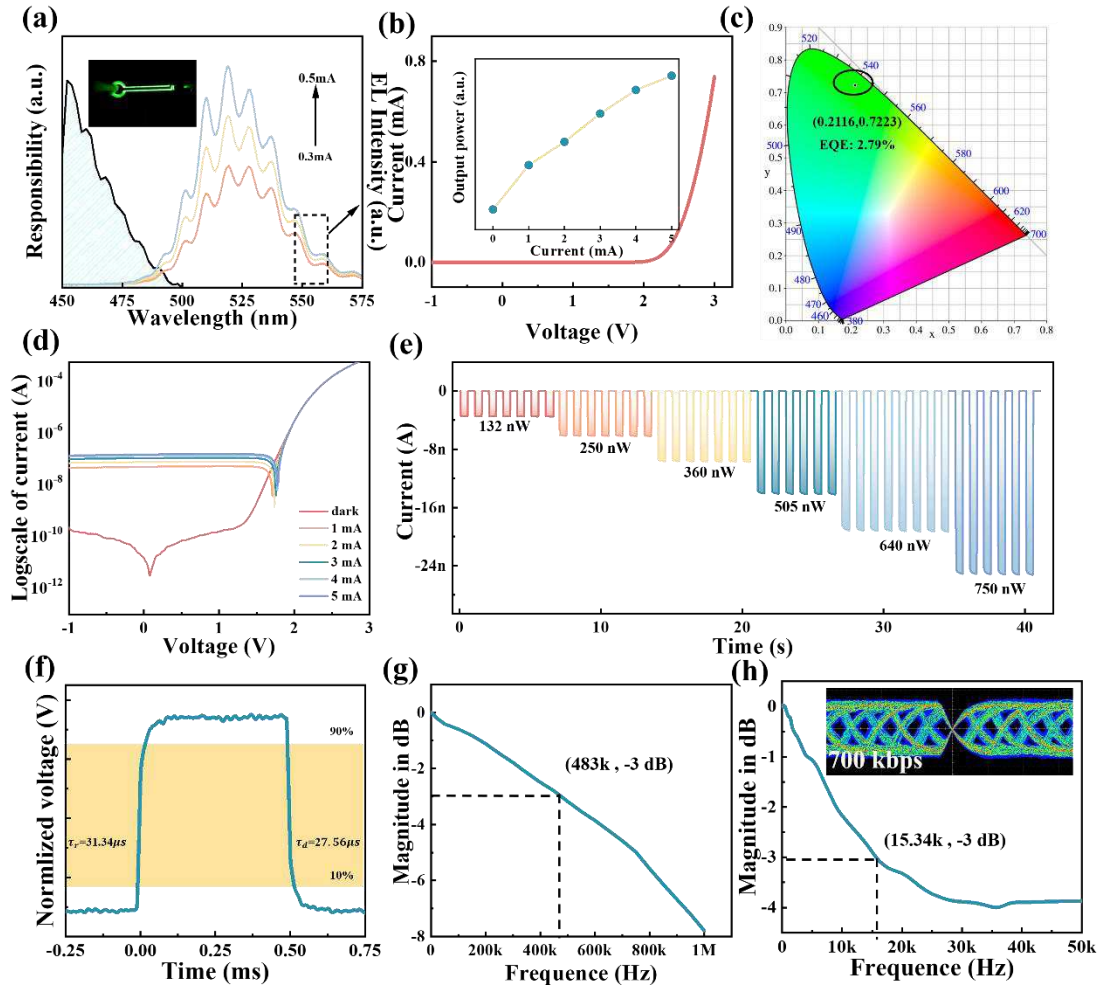

Fig. 2 (a) Driven current-related EL spectra and normalized spectral sensitivity. The insert shows the CCD images of the devices in the working state. (b) IV characteristics of the emitter; the inset shows the driven current-related EL intensity. (c) Coordinates of the CIE

1931 chromaticity diagram. (d) IV curves of the receiver under different light power conditions. (e) Optical response current under different light power conditions. (f) Dynamic photocurrent response of the receiver. (g) -3dB diagram of the emitter and (h) -3dB diagram of the receiver. The insert shows the eye diagram of the devices. The insert shows the eye diagram of individual communication unit.

Crosstalk between adjacent devices will highly influence the on-chip data transmission to achieve simultaneous multichannel transmission [32, 33]. With a misaligned bandwidth and relatively significant refractive index difference, Si is opaque to the light emitted by the GaN devices, effectively avoiding crosstalk generated through the substrate. Additionally, the light radiation emitted by the devices vertically towards the substrate and into free space can be neglected, as there is no mirror to deflect its optical path. The main in-plane crosstalk should primarily arise from light radiation along the direction parallel to the substrate from nearby emitters. Since the distance of the nearby coupled structure is 1 mm, and the total height of the stacked layers during the fabrication process is approximately 5 μm, which is much smaller than the distance. Therefore, the emitter can be approximated as a uniform line light source formed by multiple point light sources arranged in a row. For each single-point light source, it radiates uniformly in space, as shown in Fig. 3(a). If the center of the surface element dS is taken as the coordinate origin, dS receives light radiation from the point light source S. The distance from the point light source S to the surface element dS is denoted as r. The coordinates of point light source S in the 2D plane are (x, y), and the angle θ is the angle between the optical axis of the point light source beam and the normal plane of the surface element. The solid angle subtended by the surface element dS for the point light source can be denoted as:

$$d\Omega = \frac{dS cos\theta}{r^2} \tag{1}$$

Where cos θ can be expressed as the following formula:

$$cos\theta = \frac{|y|}{r} = \frac{|y|}{\sqrt{x^2+y^2}} \tag{2}$$

The luminous flux caused by the point light source within this solid angle can be denoted as:
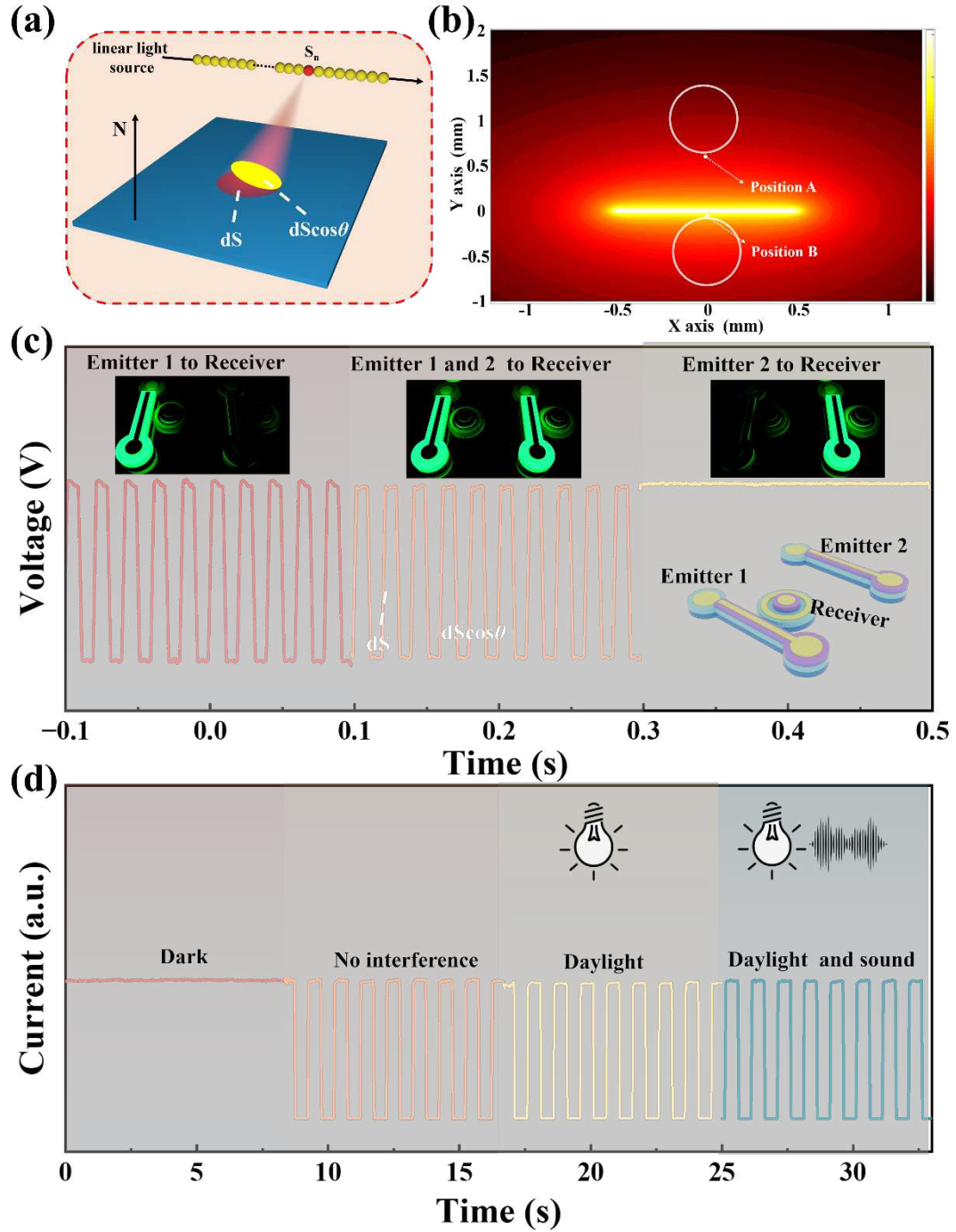
Fig. 3 (a) Illuminance contribution model of a point light source in space. (b) The spatial light intensity distribution of the line light source is shown on a log scale; the mark position indicates the receiver locations. Internal signal crosstalk experiment: (c) work without the interference of adjacent device, work with the interference of adjacent device, and receive only adjacent interference. (d) Environmental signal crosstalk experiment, The photocurrent comparison in four conditions (dark, without any interference, under the daylight, and the daylight with sound interference)

$$d\phi = Id\Omega \tag{3}$$

The entire luminous flux is projected onto the surface element dS, so the equation gives the illuminance on the surface element:

$$E = \frac{d\Phi}{dS} = \frac{I}{r^3}|y| \tag{4}$$

Taking the midpoint of the light source as the coordinate origin, with the direction towards one endpoint as the positive x-axis, let the coordinates of the center of the surface element be (x0, y0). The distance r from the extremely short strip uniform light source with a length of dL along the x-axis to the surface element dS can be expressed as:

$$r = \sqrt{(x - x_0)^2 + y_0{}^2} \tag{5}$$

Extending the point light source to a uniform line light source, the line radiation density can be denoted as Iline and its corresponding illuminance contribution can be expressed as:

$$dE = \frac{I_{line}}{r^3}|y_0|dx \tag{6}$$

Integrating the illuminance concerning x gives the total illuminance contribution of the line light source with length L to a surface element as:

$$E_{all} = \int_{-\frac{L}{2}}^{\frac{L}{2}} \frac{I_{line}|y_0|}{[(x - x_0)^2 + y_0{}^2]^{\frac{3}{2}}} dx \tag{7}$$

Based on the equations above, the calculated spatial light intensity distribution of the emitter is shown in Fig. 3(b). It can be observed that the light intensity distribution of the line light source undergoes significant attenuation as the distance from the light source increases. Together with the emitter, two positions for receivers, as determined by the SEM results, are marked and named Position A and B. The intensity for position B is significantly higher (four orders of magnitude) than that for position A. This demonstrates that a unit distance of 1 mm is sufficient to avoid crosstalk within the chip. The multi-input single-output experiment was used to experimentally verify the low crosstalk characteristics of the chip during data transmission. As shown in the insert figure of Fig.3(c), during the experiment, Emitter 1 (with a 50 Hz square signal) and Emitter 2 (with a 10 Hz square signal) at the same signal intensity served as the emission end and the signal was sent to the receiver in the middle. The waveform data in Fig. 3(c) indicate that emitter 1 and the receiver can form a signal channel well, and the additional interference signal introduced

by emitter 2 has a negligible effect on the communication performance of the coupled device. Moreover, there is no signal channel between emitter 2 and the receiver. These results align with the previous analytical calculations and simulation outcomes. Apart from the internal crosstalk, the environmental influence on the chip was also measured and is shown in Fig. 3(d). For a fixed communication channel, the waveform of optical communication under three conditions: no interference, sunlight interference only, and both sunlight and sound interference. It is evident from Fig. 3(d) that waveforms are nearly the same under sunlight conditions and sunlight with added noise interference, respectively. These results demonstrate that our device is insensitive to sunlight and sound signals. This is beneficial for the simultaneous low-interference transmission of multiple optical signals on the chip. To further verify the long-term operational stability and reproducibility of the disk as the sensing end, we conducted periodic signal transmission tests on a single device for a total duration of approximately 100 seconds (see details in Fig. S5). Three segments of about 2 s each were randomly selected, and by observing the output photocurrent signal waveforms, we found that the signal waveform exhibited good stability and reproducibility.

2.4 Demonstration of multichannel data transmission system

Based on the discussion above, we designed a communication system for transmitting text and images. As shown in Fig. 4(a), the introductory text and image information are encoded and output by the microcontroller, then amplified by the first-stage amplifier, and transmitted to any two pairs of communication units on the integrated optoelectronic chip. The output of the single device is further amplified by the second-stage amplifier and sent via serial communication to the PC, where the information is decoded and reconstructed. The same module drives both stages of amplification. The actual system image and the actual signal transmitted in the system are shown in Figs. S6 and S7. The signal output by the integrated optoelectronic chip passes through the amplifier, which has been reconfigured into a two-stage amplification system based on actual transmission conditions. Fig. 4(b, c) shows the waveform of the transmitted text signal, where the text signal uses defined high and low-level points to represent "0" and "1," and the information is decoded using the ASCII code. The information decoded from the waveform in the figure is "NJUPT20012616". With a similar method, image information can also be transmitted to

the chip. The basic principle of image transmission is first to convert the original image into grayscale and then perform 256-level quantization. After the receiving end receives all the sampled data, the image is restored and then processed with pseudocolor. The original image used for image signal transmission is shown in Fig.4(d). Fig. 4 (e-g) shows the pseudocolor images restored after averaging the signal at five different data rates, with symbol durations of 100 μs, 500 μs, and 1 ms, respectively. Although the restored images are generally similar to the original image, it is observed that as the symbol duration increases, the restored image becomes clearer, with more distinct details and sharper edges.
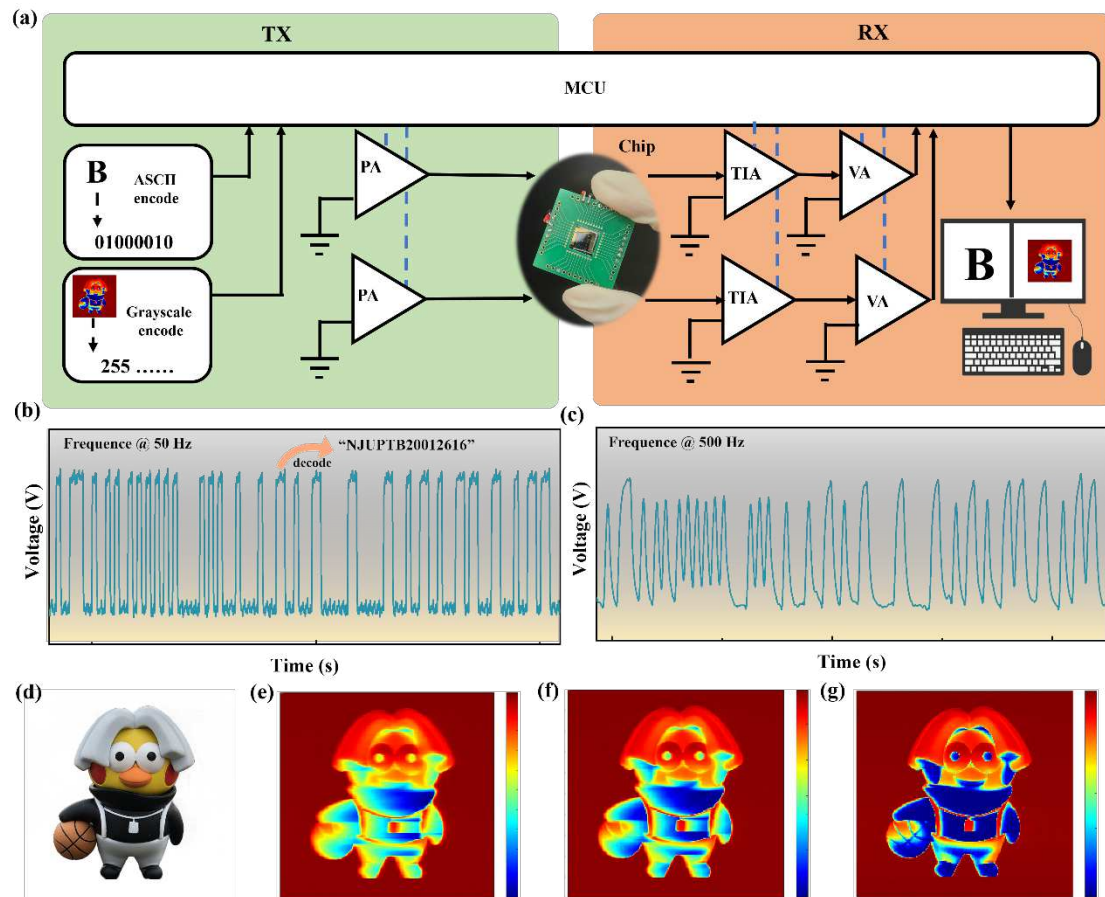

Fig. 4 (a) The diagram of the communication system, (b, c). The text signal patterns for different square wave frequencies of 50 Hz and 500 Hz. (d) for original image signal transmission. (e-g) show the restored pseudocolor images with varying durations of symbol (100 μs, 500 μs, and 1 ms, respectively).

3. Conclusion

In this work, we propose and demonstrate a Si-based integrated optoelectronic chip capable of waveguide-free, low-crosstalk, and multichannel optical signal transmission. The chip integrates a 15-pair array of InGaN/GaN MQW devices with square emitters and circular receivers. The InGaN/GaN devices operate with emission spectra ranging from 475 nm to 575 nm and optical response spectra ranging from 350 nm to 500 nm. For an individual unit, rise and decay times of 31.34/27.56 μs, a system communication bandwidth of 15.34 kHz, and a data rate exceeding 0.7 Mbps are obtained. The channels are individually isolated and insensitive to inter-channel and environmental interferences, including extraneous sound signals and daylight. The overall data rate of the chip can be estimated to exceed 10.5 Mbps. Through detailed characterization and verification via simulations and experiments, we confirm the feasibility of on-chip communication. Furthermore, the communication system built upon this chip successfully transmits and decodes both text and image signals with minimal interference from the environment. These results demonstrate the great potential of silicon-based integrated optoelectronic chips for scalable, low-interference optical communication systems.

4. Materials and methods

4.1 Fabrication of the communication unit

Similar to our previous work, the epitaxial wafer used in the device array of this study is grown by the metal-organic vapor phase epitaxy (MOVPE) method. The layers of the wafer, from top to bottom, consist of a 0.4 μm player made of AlGaN/GaN, a 0.35 μm Active layer of InGaN/GaN, 2.8 μm of n-GaN, a 1.5 μm Buffer layer made of AlN/AlGaN/uGaN, and a 1500 μm silicon substrate. The integrated optoelectronic chip in this study is realized through photolithography, inductively coupled plasma (ICP) etching, and metal deposition processes. Firstly, the structures of the p-type area are patterned on the photoresist layer using photolithography. The epitaxial layer, with a thickness of approximately 2.5 μm, is then etched to the n-GaN layer by ICP etching, with the photoresist layer serving as a mask. Secondly, the n-type area was redefined using the photoresist layer, followed by ICP etching to a thickness of 3.0 μm on the silicon substrate layer and the removal of residual photoresist. Finally, the photoresist layer is again patterned by photolithography. The p-electrode and n-electrode are prepared on the n-GaN and p-GaN layers by electron beam evaporation, and the

residual photoresist is removed using an acetone solution. The electrode material is composed of 20 nm nickel and 100 nm gold.

4.2 Fabrication of the communication unit

The device morphology includes scanning electron microscopy (SEM, SU-8010) and CCD images (Zeiss optical microscope). The analysis results involved in elemental characterization include Powder XRD (Bruker D8 Advance diffractometer, Cu Kα radiation, λ = 1.54056 A) and Raman spectroscopy (Raman, Bruker RAM), where the Raman spectra were obtained using a 532 nm laser and a 600-line/mm grating. During optoelectronic characterization, the following instruments were mainly used: source meter (for power supply and low-frequency signal acquisition, Keysight B2901), signal generator (for generating specific frequency signals, RIGOL DG4062), oscilloscope (for rise/fall edge and transmission signal capture, Tektronix TDS3052B), and spectrometer (for EL spectrum, Acton SP2500i).

Acknowledgments

Author contributions

F. Q., X. W., and G. Z. proposed the idea and the conceptual design. Y. W. and Q. J. guided this work. J. W. and X. L. carried out the experimental setup, system optimization, and measurements. D. Y. assisted with the experiments. J. W. and X. Lu wrote the paper. All authors contributed to revising the paper.

Data availability

The data are available from the corresponding authors upon reasonable request.

Conflict of interest

The authors declare no competing interests.

Supplementary information

Property characterization of the device and physical diagram of the prototype system.

Reference

1. H. Zhao, M. Feng, J. Liu, X. Sun, T. Tao, Q. Sun and H. J. N. Yang, **12** (1), 111-118 (2023).
2. Z. Gao, T. Jiang, M. Zhang, H. Wu, M. J. L. S. Tang and Applications, **14** (1), 60 (2025).
3. A. H. Atabaki, S. Moazeni, F. Pavanello, H. Gevorgyan, J. Notaros, L. Alloatti, M. T. Wade, C. Sun, S. A. Kruger, H. Meng, K. Al Qubaisi, I. Wang, B. Zhang, A. Khilo, C. V. Baiocco, M. A. Popović, V. M. Stojanović and R. J. Ram, Nature **556** (7701), 349-354 (2018).
4. C. J. Chung, X. Xu, Z. Pan, F. Mokhtari-Koushyar, R. Wang, H. Yan, H. Subbaraman and R. T. Chen, Journal of Lightwave Technology **36** (9), 1568-1575 (2018).
5. X.-X. Wang, G. Zeng, Q.-J. Yu, L. Shen, C.-Y. Shi and H.-L. Lu, Nanoscale **16** (11), 5504-5520 (2024).
6. Y. Xie, J. Wu, S. Hong, C. Wang, S. Liu, H. Li, X. Ju, X. Ke, D. Liu and D. Dai, Nanophotonics **13** (12), 2051-2073 (2024).
7. Z. Xu, B. Tian, X. Fan, J. Wei, Z. Tan, Q. Lv and C. Zheng, Microwave and Optical Technology Letters **66** (4), e34046 (2024).

8.   R. Gupta, A. Kumar, M. Kumar, R. Singh, A. Gehlot, P. S. Pandey, N. Yadav, K. Pandey, A. Yadav, N. Gupta, R. Brajpuriya, S. Kumar, A. S. Verma, T. Kumar, Y. Wu, Z. Hongyu, A. Biswas, A. Mittal, A. Mondal and R. O. Ivanovich, Nano Materials Science (2024).

9.   K. Liao, Y. Lian, M. Yu, Z. Du, T. Dai, Y. Wang, H. Yan, S. Wang, C. Lu, C. T. Chan, R. Zhu, D. Di, X. Hu and Q. Gong, Nature Photonics (2025).

10. R. Kumar, S. K. Saha, A. Kuchuk, Y. Maidaniuk, F. M. de Oliveira, Q. Yan, M. Benamara, Y. I. Mazur, S.-Q. Yu and G. J. Salamo, Applied Surface Science **542**, 148554 (2021).

11. Y. Chen, K. Jiang, B. Wang, K. Liu, X. Wang, J. Ben, S. Zhang, S. Lu, Y. Chen, Y. Jia, M. Liu, X. Sun and D. Li, Applied Physics Letters **124** (16) (2024).

12. J. Feng, Z. Wang, M. Zhanghu, X. Zhang, Y. Shen, J. Yang, Z. Li, B. Chen, T. Wang, X. Chen and Z. Liu, Microsystems & Nanoengineering **10** (1), 85 (2024).

13. T. Jia, M. Zhang, G. Zhang, S. Hang, C. Chu, Y. Zhang, and Z.-H. Zhang, Opt. Express **31** (2), 2931-2941 (2023).

14. K. H. Li, Y. F. Cheung, W. S. Cheung and H. W. Choi, Applied Physics Letters **107** (17) (2015).

15. Y. Wang, G. Zhu, W. Cai, X. Gao, Y. Yang, J. Yuan, Z. Shi and H. J. A. P. L. Zhu,   **108** (16) (2016).

16. F. Qin, X. Lu, X. Wang, C. Guo, J. Wu, X. Fan, M. Jiang, P. Wan, J. Lu, Y. Wang and G. Zhu, Chip **3** (4) (2024).

17. R. He, Y. Song, N. Liu, R. Chen, J. Wu, Y. Wang, Q. Hu, X. Chen, J. Wang and J. J. A. P. Li,   **9** (7) (2024).

18. Y. Miyoshi, Y. Fukazawa, Y. Amasaka, R. Reckmann, T. Yokoi, K. Ishida, K. Kawahara, H. Ago and H. Maki, Nature Communications **9** (1), 1279 (2018).

19. W. Pan, L. Wang, J. Tang, H. Huang, Z. Hao, C. Sun, B. Xiong, J. Wang, Y. Han, H. Li, L. Gan and Y. Luo, Light: Science & Applications **14** (1), 48 (2025).

20. K. Fu, X. Gao, Z. Ye, J. Li, X. Ji and Y. Wang, Optics Letters **47** (11), 2614 (2022).

21. X. Gao, T. Yu, T. Chang, D. Wu, M. Xie, N. Chi, Y. Wang and Z. Shi, Optics Express **32** (6), 10732 (2024).

22. X. Gao, D. Wu, T. Xie, J. Yuan, M. Xie, Y. Wang, H. Zhao, G. Zhu and Z. Shi, Chip **3** (4), 100113 (2024).

23. M. Hosseini and S. Mohajerzadeh, IEEE Electron Device Letters **40** (10), 1690-1693 (2019).

24. S. Çörekçi, S. Dugan, M. K. Öztürk, S. Ş. Çetin, M. Çakmak, S. Özçelik and E. Özbay, Journal of Electronic Materials **45** (7), 3278-3284 (2016).

25. P. J. Pauzauskie, D. Talaga, K. Seo, P. Yang and F. Lagugné-Labarthet, Journal of the American Chemical Society **127** (49), 17146-17147 (2005).

26. M. Naddaf, M. Ahmad and N. Salman, Nuclear Instruments and Methods in Physics Research Section B: Beam Interactions with Materials and Atoms **548** (2024).

27. W. Song, X. Wang, H. Chen, D. Guo, M. Qi, H. Wang, X. Luo, X. Luo, G. Li and S. J. J. o. M. C. C. Li,   **5** (44), 11551-11558 (2017).

28. T. Xu, X. Fan, G. Zhu, F. Qin, P. Wan, K. Tang, C. Kan, D. Shi, X. Fang and M. J. A. O. M. Jiang,   **12** (19), 2400237 (2024).

29. X. Zou, X. Zhang, Y. Zhang, Q. Lyu, C. W. Tang and K. M. J. A. A. E. M. Lau,   **2** (3), 719-724 (2020).

30. F. Varghese and P. J. W. P. C. Sasikala, **129** (4), 2291-2318 (2023).

31. H. Tong, Z. Yang, S. Wang, Y. Hu, O. Semiari, W. Saad, C. J. F. i. c. Yin and networks, **2**, 734402 (2021).

32. Z. Liu, S. Gao, Z. Lai, Y. Li, Z. Ao, J. Li, J. Tu, Y. Wu, W. Liu, Z. J. L. Li and P. Reviews, **17** (4), 2200536 (2023).

33. H. Jiang, Y. Hu, X. Gao, T. Wei, N. Li, Q. Zhang, W. Jia, L. Chen, X. Guo and Y. J. A. F. M. Lei, 2500628 (2025).

Supplementary Files

This is a list of supplementary files associated with this preprint. Click to download.

- SI.docx